Estimating and Eliminating the Excitation Errors in Bipolar Gradient Composite Excitations Caused by Radiofrequency-Gradient Delay: Example of Bipolar Spokes Pulses in Parallel Transmission

Desmond H.Y. Tse,[1]* Christopher J. Wiggins,[2] and Benedikt A. Poser[1]

Purpose: To eliminate a slice-position–dependent excitation error commonly observed in bipolar-gradient composite excitations such as spokes pulses in parallel transmission.

Theory and Methods: An undesired timing delay between subpulses in the composite pulse and their bipolar slice-selective gradient is hypothesized to cause the error. A mathematical model is presented here to relate this mismatch to an induced slice-position–dependent phase difference between the subpulses. A new navigator method is proposed to measure the timing mismatch and eliminate the error. This is demonstrated at 7 Tesla with flip-angle maps measured by a presaturation turbo-flash sequence and in vivo images acquired by a simultaneous multislice/echo-planar imaging (SMS-EPI) sequence.

Results: Error-free flip-angle maps were obtained in two ways: 1) by correcting the time delay directly and 2) by applying the corresponding slice-position–dependent phase differences to the subpulses. This confirms the validity of the mathematical description. The radiofrequency (RF)-gradient delay measured by the navigator method was of 6.3 μs, which agreed well with the estimate from flip-angle maps at different delay times. By applying the timing correction, accurately excited EPI images were acquired with bipolar dual-spokes SMS-2 excitations.

Conclusion: An effective correction is proposed to mitigate slice-position–dependent errors in bipolar composite excitations caused by undesired RF-gradient timing delays. **Magn Reson Med 78:1883–1890, 2018.**

Key words: ultra-high-field MR; parallel transmission; excitation errors; bipolar gradient spokes pulses; SMS-pTX; EPI

INTRODUCTION

Multichannel parallel transmission (pTx) of spokes pulses (1) has been demonstrated as a promising way to mitigate flip-angle inhomogeneity in 2D or slab imaging at 7 Tesla (T) (1,2) and 9.4T (3–5). In excitation k-space, the spokes pulses trajectory follows a series of lines ("spokes") defined by the slice-selective gradient, at positions determined by intermittent x-y gradient blips. These trajectories resemble an echo-planar imaging (EPI) readout trajectory with the k-space lines parallel to the slice direction instead of the readout direction. In EPI, any phase inconsistency or k-space misalignment between the odd and even readout lines, for example, caused by a delay between the gradient and signal readout, leads to the well-known Nyquist ghosting (6). Similar misalignment and phase errors also occur in bipolar composite pulses between the radiofrequency (RF) subpulses and cause unrecoverable excitation errors, that is, mismatches between the achieved flip-angle spatial distribution and the expectation from the pulse calculation. It has been reported that strong eddy currents cause errors in spokes excitations, which can be remedied by mapping the actual gradient response and applying a compensatory time-varying phase to the RF pulse (5). In modern scanner systems, where effects of eddy current are usually small because of the precisely calibrated pre-emphasis, errors in bipolar spokes excitations are still observed.

Apart from eddy currents, excitation errors in bipolar spokes pulses are also known to be caused by a timing delay between the slice-selective gradient and the transmitted RF (7–9), analogous to the odd-even delays in EPI readouts described above. Similar errors caused by RF-gradient delay have also been observed in 2D selective pulse with spiral excitation trajectory (10–12). k-space trajectory mapping methods (13,14) can be used for corrections during pulse design to mitigate errors (12). These methods are excellent in measuring the trajectory distortion caused by eddy current and relative delays between gradient axes, but the absolute delay between the RF transmission and the gradient can only be inferred because they only measure the timing relationship between the gradient and the receive chain. A systematic difference has been shown in the RF-gradient delay estimated by a trajectory mapping method (13) and another method based on the distortion on the pattern excited by a 2D selective pulse (10). A total phase mapping method, which was proposed for correcting the phase errors attributed to eddy current and B_0 inhomogeneity, has the potential to implicitly compensate the phase errors caused by the RF-gradient delay (7).

[1]Faculty of Psychology and Neuroscience, Maastricht University, Maastricht, The Netherlands.

[2]Scannexus BV, Maastricht, The Netherlands.

*Correspondence to: Desmond H.Y. Tse, Ph.D., Faculty of Psychology and Neuroscience, Maastricht University, P.O. Box 616, 6200MD Maastricht, The Netherlands. E-mail: desmond.tse@maastrichtuniversity.nl

Received 26 August 2016; revised 23 November 2016; accepted 23 November 2016

DOI 10.1002/mrm.26586
Published online 26 December 2016 in Wiley Online Library (wileyonlinelibrary.com).

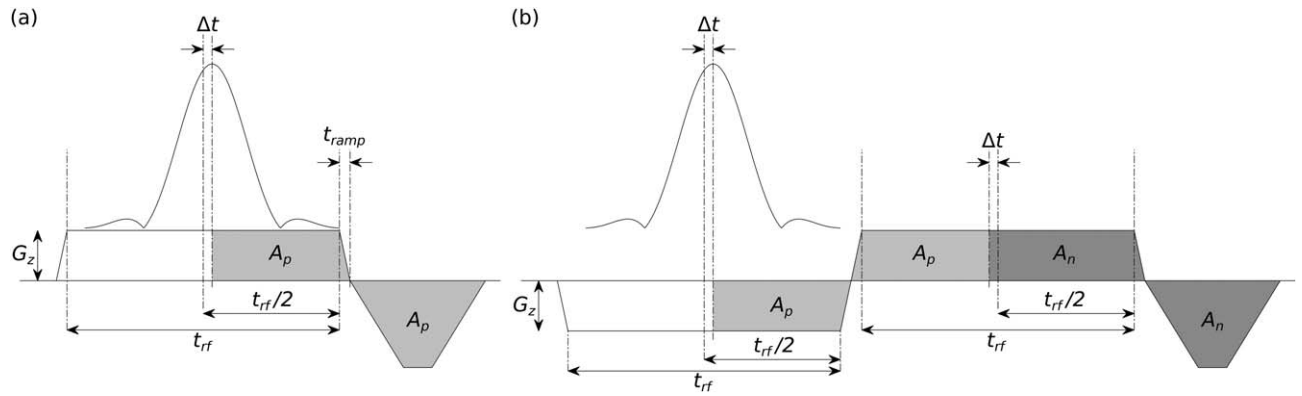

FIG. 1. Schematic of a bipolar spokes excitation pulse together with their slice-selective and rephasing gradient lobes. The subpulses are symmetric *sinc* pulses in this case. G_z is the required slice-selective gradient amplitude, t_{rf} is the duration of the *sinc* pulse, t_{ramp} is the ramp time of the slice-selective gradient, and Δt is the delay between the playout of the *sinc* pulse and the slice-selective gradient. Panel (**a**) shows the case of the odd subpulses in which the slice-selective gradient has the opposite polarity to the rephasing lobe. The required rephasing moment in this case is A_p; (**b**) shows the case of the even subpulses in which the slice-selective gradient and the rephasing lobe have the same polarity. In this case, the required rephasing moment is A_n. They demonstrate how a delay of Δt between the symmetric *sinc* pulse and its slice-selective gradient results in different required slice rephasing gradient moment. This leads to a slice-dependent phase difference between the (**a**) positive and (**b**) negative lobes spokes subpulses given by Equation [4].

In this study, we first present a mathematical description for the effect of this delay on bipolar-gradient composite excitations. We then propose a navigator approach, similar to the total phase mapping method (7), to estimate the delay and show two effective ways of eliminating these errors in bipolar composite pulses. Finally, we validate the proposed method by examining both flip-angle maps and EPI images obtained with and without the delay correction.

THEORY

Slice-selective excitation pulses require a rephasing gradient to remove the through-slice phase dispersion induced by the slice-selective gradient (15). When there is delay of Δt between a symmetric pulse (typically a *sinc* pulse, as assumed here) and its slice-selective gradient, the required rephasing gradient moment, A_p, as demonstrated in Figure 1a, is shown by Equation [1]:

$$A_p = \frac{G_z}{2}(t_{rf} + t_{ramp} - 2\Delta t), \qquad [1]$$

where G_z is the required slice-selective gradient amplitude, t_{rf} is the duration of the *sinc* pulse, t_{ramp} is the ramp time of the slice-selective gradient, and Δt is the delay between the playout of the *sinc* pulse and the slice-selective gradient.

For multiple-subpulse spokes excitation with bipolar gradients, Equation [1] is correct for all subpulses that have their slice-selective gradient in the opposite polarity to the rephasing lobe, namely, the odd set of subpulses, as shown in Figure 1a. For the even set of subpulses, where both the slice-selective and rephasing gradient lobes are in the same polarity, the required rephasing moment, A_n, is given by Equation [2]:

$$A_n = \frac{G_z}{2}(t_{rf} + t_{ramp} + 2\Delta t), \qquad [2]$$

as in Figure 1b.

When $\Delta t \neq 0$, the rephasing moments required by the two sets of subpulses cannot be satisfied by a common gradient lobe. This leads to two types of residual phase errors: First, the through-slice phase dispersions induced by the two sets of subpulses differ by Equation [3]:

$$\delta\phi = 2\gamma G_z \Delta t \Delta z = 4\pi BW \Delta t, \qquad [3]$$

where γ is the gyromagnetic ratio, Δz is the slice thickness, and BW is the bandwidth of the RF pulse; Second, at the center of the slice cross-section, the two sets of subpulses have a phase difference given by Equation [4]:

$$\Delta\phi = 2\gamma G_z \Delta t z = 4\pi BW \Delta t \frac{z}{\Delta z} = \delta\phi \frac{z}{\Delta z}, \qquad [4]$$

where z is the position of the center of the slice from the gradient isocenter.

Although the difference in through-slice phase dispersion, $\delta\phi$, cannot be corrected by a common rephasing gradient lobe, its effect is generally small, because BW is typically in the range of kHz and Δt is expected to be in the order of μs in a well-calibrated MR system, leaving $\delta\phi$ in the order of 0.1 radians. In contrast, the phase difference between the two sets of subpulses, $\Delta\phi$, which scales linearly with the slice position z, can be a factor 10 larger than $\delta\phi$ and in the order of π radians, for example, for a 2-mm-thick slice at 20 mm from the isocenter. When this amount of phase difference is not accounted for, the desired flip-angle homogenization cannot be achieved. Unlike the first type of phase errors, which can only be corrected by eliminating the delay Δt, the effect of this phase difference $\Delta\phi$ can also be compensated by adding the extra slice-dependent phase difference between the set of odd and even subpulses according to Equation [4].

METHODS

Imaging experiments were performed on a MAGNETOM 7 T MR scanner (Siemens Medical Systems, Erlangen,

Germany) with a whole-body gradient set (SC72; maximum amplitude, 70 mT/m; maximum slew rate, 200 T/m/s) and using an eight-channel transmit/32-channel receive head coil (Nova Medical, Wilmington, MA, USA) in parallel transmission mode (step 2.3, 1 kW per channel). All experiments were carried out in the vendor-provided "protected mode," which ensures specific absorption rate (SAR) safe operations at a safety margin of approximately a factor of 2.5 higher than the worst-case local SAR derived from electromagnetic models. All in vivo experiments were approved by the local ethics committee and performed in accord with internal safety guidelines after obtaining written informed consent. To confirm generality of the findings, a similar set of phantom experiments was performed on a 9.4T human MRI scanner by the same vendor with a head gradient set (AC84-mk2; maximum amplitude, 80 mT/m; maximum slew rate, 333 T/m/s) and a custom 16-channel transmit/31-channel receive coil (16).

Two-spoke pulses were calculated in a slice-by-slice fashion with B_0 inhomogeneity correction as described in Tse et al. (4), with a subpulse spacing of 1.36 ms (ie, a total pulse duration of 2.72 ms). For RF pulse calculation, a B_0 map was obtained using a dual-echo 3D gradient-recalled echo sequence, and the B_1^+ sensitivity mapping was performed with a transmit phase-encoded (17), T_2 and T_2^* compensated version of DREAM sequence (18) (for details on the calibration scan parameters, see Tse et al. (19)). The flip-angle spatial distributions of the two-spoke pulses were mapped by the presaturation turbo-flash FLASH (PreSat-TFL) sequence (20) in which the spokes pulses were used as the saturation pulse with a target flip angle of 45°. Images were acquired in the transversal slice direction. In order to avoid any influence of a nonideal slice profile, the saturation slice thickness in the PreSat-TFL measurements was set to 3.0 mm whereas the imaging slice thickness was 1.5 mm. The *sinc* pulse, which was used in the bipolar spokes experiments, had a bandwidth-time-product (BWTP) of 4.0. With this set of slice thickness, BWTP and the subpulse spacing, the required G_z, t_{rf} and t_{ramp} (Figs. 1 and 2) were 32.62 mT/m, 960 μs, and 200 μs, respectively. The navigator described later in this section was implemented into the saturation pulse of the PreSat-TFL sequence to estimate the time delay Δt.

In order to correct for the errors introduced by the RF-to-gradient time delay Δt, all our sequences that use spokes pulses have been modified to allow the starting time of the spokes subpulses relative to their slice-selective gradient to be adjusted from the protocol in 1-μs increments, which is the precision allowed by scanner. As a demonstration of the excitation errors caused by the time delay Δt, a series of flip-angle maps from the same set of bipolar two-spoke pulses were acquired using PreSat-TFL at 12 slice positions (ie, $z = \{-54.0, -45.0, -36.0, -27.0, -18.0, -9.0, 0.0, 9.0, 18.0, 27.0, 36.0, 45.0\}$ mm in Eq. [4]) and with 21 different relative starting times between the subpulses and their slice-selective gradient (from −15 μs to 5 μs in steps of 1 μs). This set of flip-angle maps was used to estimate the actual time delay Δt by plotting the normalized root means square errors (NRMSE) against the applied time shift and choosing the time point when the NRMSE is minimum and closest to the predicted NRMSE value from the RF pulse optimization. The estimated Δt value was then checked against the estimation from the navigator measurements described in the next paragraph. Using the same set of slice and RF parameters, this whole set of the bipolar flip-angle maps were simulated using the Bloch equation.

The flip-angle maps at the same slice positions and spokes locations were also acquired with fly-back slice-selective gradients, without modification of the relative RF-gradient starting time. In order to accommodate the rewinding lobe in the fly-back setting, the subpulse spacing was increased to 2.38 ms. The same set of complex RF scaling factors as in the bipolar case was used. The BWTP of the subpulse used in the fly-back setting was 3.3 with $t_{rf} = 880$ μs, $t_{ramp} = 180$ μs, $G_z = 29.36$ mT/m, and a total pulse duration of 3.62 ms. The estimated time delay Δt was used to calculate the slice-position–dependent phase shifts between the sets of odd and even subpulses according to Equation [4] ($2\gamma G_z = 0.01745$ rad/mm/μs), and the results were used to generate a new set of spokes pulses with these phase shifts removed. For comparison to the time-shift–corrected bipolar pulses, this new set of slice-phase-shifts–corrected bipolar pulses was also mapped at the same slice positions (again without modification of the relative RF-gradient starting time).

A dual-echo navigator as shown in Figure 2 can be inserted between the final slice-selective and the slice-rephasing gradient lobes of the spokes pulse to measure the delay Δt. The navigator is applied in the same logical slice-selective gradient axis; hence, it is also suitable for oblique imaging slices in the presence of slightly different delays on the physical gradient components. The two readout gradients in the navigator are the same as the bipolar slice gradient lobes in the spokes pulse, that is, on the same axis and with the same G_z, t_{rf} and t_{ramp} values. Two echoes are acquired in both readout gradient polarities to cancel out any error attributed to the time delay between the readout and the gradient, which is not necessarily the same as the RF delay. Any effect caused by the readout delay will be removed by averaging Δt estimated from the two echoes. In order to measure the clean echoes from one of the spokes subpulses only, the navigator is run twice, each time playing out only one of the subpulses: once with the positive slice-selective lobe subpulse, and once with the negative slice-selective lobe subpulse. In the absence of a readout delay, the echoes from the RF pulse that was played out in the positive slice-selective lobe with a delay of Δt are shifted from the central point of the readout by $+\Delta t$ in the positive readout lobe and by $-\Delta t$ in the negative readout lobe, and vice versa for the RF subpulse played out in the negative slice-selective lobe. The two situations are shown by the dotted and solid lines in Figure 2c. The navigator was run for all 12 slice positions. The signals from all the receive channels were first combined by sum-of-squares and then averaged across the slices. The receive-combined and slice-averaged signals were upsampled by a factor of 10 and the time when the echoes reach the

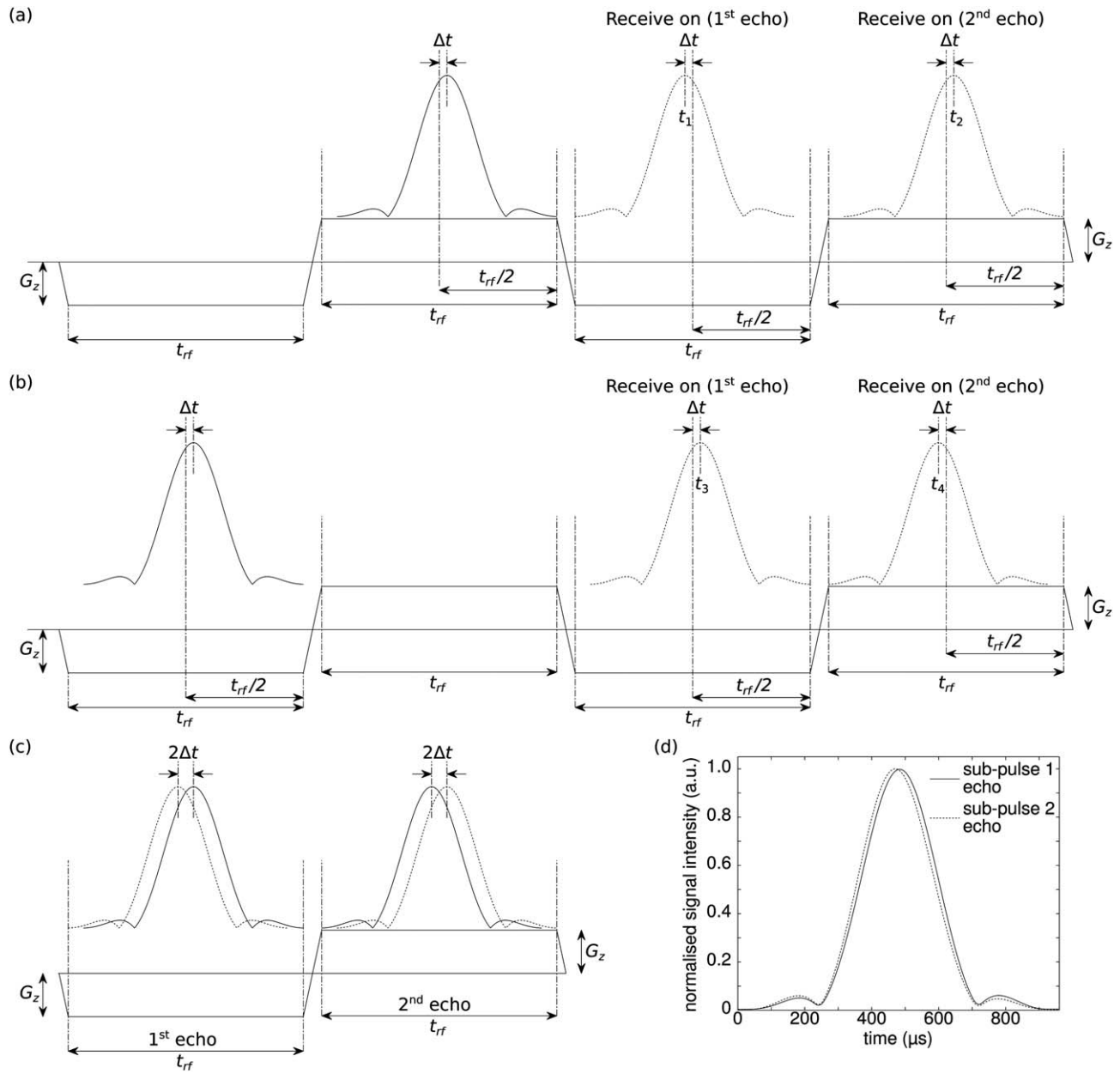

FIG. 2. Schematic of a two-step dual-echo navigator that can be used to measure Δt. The navigator is inserted between the last slice-selective gradient lobe of the spokes pulse and its rephasing gradient lobe. The readout gradients of the navigator are exactly the same as those used as the slice-selective gradients in the spokes pulse. (**a**) First step: Only the last subpulse (solid line) is played out. The delay Δt causes the signals (dotted line) of the first and second echoes to shift from the center of the readout by $-\Delta t$ and $+\Delta t$, respectively. t_1 and t_2 are the time when the signals of the first and second echoes reach the maximum, respectively. (**b**) Second step: Only the second last subpulse (solid line) is played out. With the same delay Δt, now the first and second echoes are shifted in the opposite direction from the first step. t_3 and t_4 are the time when the signals of the first and second echoes reach the maximum, respectively. (**c**) With the sign of the time delay shown in (**a**) and (**b**), the dotted line in (**c**) represents the echo from the *sinc* pulse played out in (**a**) with a positive slice-selective gradient lobe; and the solid line represents the echo played out in (**b**) with a negative slice-selective gradient lobe. (**d**) Navigator echoes from subpulses of both gradient polarities, measured with the proposed navigator approach for direct measurement of the excitation waveforms. Any readout delays have been corrected for by using the second navigator echoes (for details, see Methods).

maximum, as indicated as t_1, t_2, t_3, and t_4 in Figure 2a and 2b, were determined. Δt is given by $(t_2 - t_1 + t_3 - t_4)/4$.

Finally, to illustrate the excitation errors and the efficacy of the proposed corrections, in vivo echo-planar images were acquired using SMS-pTX spokes excitations (4,21,22) with and without the timing correction. The same set of two-spoke pulses complex scaling factors as used in the flip-angle mapping above was multiplexed directly in the pulse sequence to form a dual-spokes simultaneous multislice (SMS-2) excitation pulse according to Equation [4] in Tse et al. (4). Attributable to the limit on the total number of RF pulses that the scanner

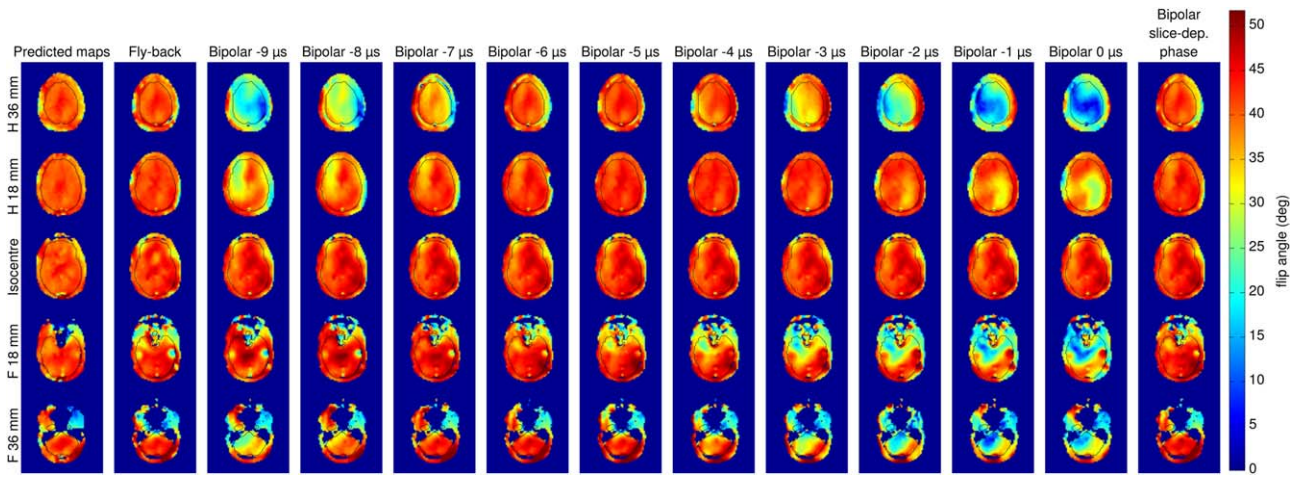

FIG. 3. Flip-angle maps of two-spoke pulses measured by PreSat-TFL. Five slice positions between –36 mm and +36 mm are displayed here. The left column is the predicted flip-angle distribution from the spokes pulse optimisation. The second column from the left shows the flip-angle maps from the fly-back spokes pulses. The next 10 columns are the flip-angle maps from the bipolar spokes pulses with the relative starting time between the subpulses and the slice-selective gradient set from –9 µs to 0 µs (left to right). The last column plots flip-angle maps from the bipolar spokes pulses with the slice-position–dependent phases corrected using Equation [4] and without any timing correction. The fly-back spokes, the bipolar spokes with –6 µs relative starting time shift, and the bipolar spokes with the slice-position–dependent phases corrected agree the best with the prediction.

can handle, six neighbouring EPI imaging slices were grouped together to share the same spokes pulse (4,23). For reference, EPI images were also acquired with fly-back spokes and in CP-mode. The EPI slice thickness was 1.5 mm and flip-angle was set to 20°. The parameters for the subpulses were: 1) bipolar: BWTP = 4.0, subpulse spacing = 2.04 ms, t_{rf} = 1.66 ms, t_{ramp} = 190 µs, G_z = 37.73 mT/m, and a total pulse duration of 4.08 ms; 2) fly-back: BWTP = 2.7, subpulse spacing = 3.10 ms, t_{rf} = 1.51 ms, t_{ramp} = 140 µs, G_z = 28.00 mT/m, and a total pulse duration of 4.89 ms; and 3) CP-mode: BWTP = 4.0, t_{rf} = 1.66 ms, t_{ramp} = 190 µs, G_z = 37.73 mT/m, and a total pulse duration of 2.04 ms.

RESULTS

Figure 3 shows the flip-angle maps of two-spoke pulses measured with PreSat-TFL at five different slice positions. Fly-back spokes (NRMSE = 0.096), bipolar spokes with –6 µs correction of the RF-gradient starting time (NRMSE = 0.093), and bipolar spokes with slice-dependent RF phase correction according Equation [4] (NRMSE = 0.091) all agree well with one another and are close to the flip-angle prediction from the pulse optimisation (NRMSE = 0.059). With the default RF-gradient timing, that is, nominal 0 µs, the slice-position–dependent excitation errors can be seen clearly. These errors depend on the relative RF-gradient timing as hypothesized, and were minimized at –6 µs. No error can be observed at the isocenter in all cases. Without the RF-gradient delay, Bloch simulations (Supporting Fig. S1) show that there is no excitation error with the default RF-gradient timing (NRMSE = 0.070). All these observations can be predicted by the model described by Equation [4]. Analogous 9.4T flip-angle maps obtained from a head-shaped phantom are shown in Supporting Figure S2. The estimated time delay on the 9.4T system was –4 µs.

The excitation errors as a function of the relative RF-gradient starting time in the bipolar excitations are plotted in Figure 4, at three different slice locations and averaged over all 12 slices (triangles). Indicated for reference are the predicted NRMSE from the pulse optimization (circle), as well as the measured NRMSE of the fly-back spokes and slice-phase corrected bipolar spoke for which good agreement is seen (all measured minimum NRMSE were within a range from 0.091 to 0.096). As observed from the flip-angle maps in Figure 3, the bipolar excitation error is time-shift invariant at the isocenter (Fig. 4a) where no erroneous phase is accumulated as per Equation [4]. For each of the off-center slice positions and the slice average, the bipolar spokes have a minimum NRMSE at –6 µs (isocenter: 0.085, –36 mm: 0.050, –54 mm: 0.126, slice average: 0.093), which are close to the NRMSE values of the fly-back spokes (0.096) and the prediction (0.059). This indicates that the errors caused by the RF-gradient timing mismatch are minimized and adequately compensated with a –6 µs shift. As seen in Figure 4b and 4c, the two example slices at 36 and 54 mm also have additional minima at time shifts other than –6 µs, following a quasi-sinusoidal behaviour with a frequency that depends linearly on the off-center slice position. This is explained by Equation [4], which shows that, for a given slice position and gradient amplitude, the error will be minimized at all time shifts when the value of the phase difference is an integer multiple of 2π.

The result of mapping the subpulses of different polarity with the proposed navigator approach is shown in Figure 2d. The measurement compensates for any errors attributed to readout delay by using the echoes from the second navigator readout with reversed gradient polarity. The time delay between the pulses (ie, navigator echoes) is found to be 12.6 µs, corresponding to a value of 6.3 µs for Δt. In addition, navigator echoes were also acquired

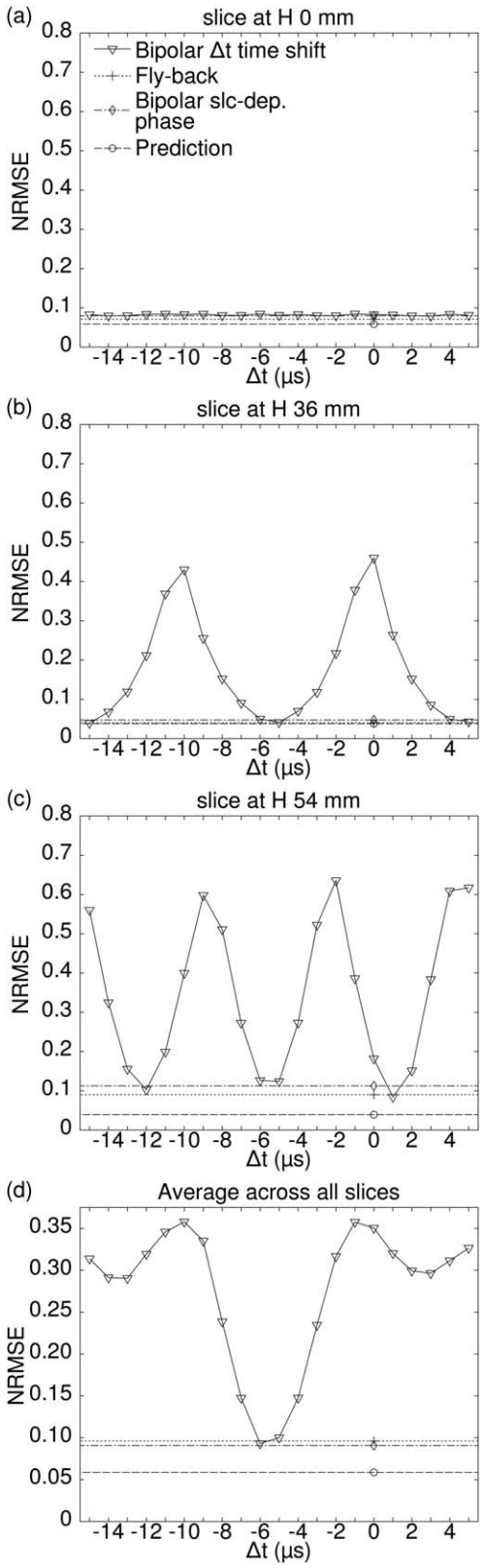

FIG. 4. NRMSE from the pulse optimization and estimated from the PreSat-TFL measured flip-angle maps of the spokes pulses in the three configurations tested (fly-back, bipolar with relative starting time adjusted, and bipolar with the slice-position–dependent phase shift corrected): (**a**) slice at the isocenter; (**b**) slice at 36 mm from the isocenter; (**c**) slice at 54 mm from the isocentre; and (**d**) averaged over all slices.

along the x- and y-axes of the gradient (ie, left-to-right and posterior-to-anterior directions) and yielded values of 2.9 and 2.2 μs, respectively, for Δt.

Figure 5 demonstrates the application of two-spoke multiband pulses in an SMS-EPI sequence with slice-acceleration factor 2. The prediction from the pulse optimization (Fig. 5a) shows a homogenized excitation pattern. Without the RF-gradient relative starting time correction, the EPI images using the bipolar two-spoke excitation pulse exhibit intensity losses in several slices away from the isocenter (Fig. 5b). The patterns of the artefacts match the excitation patterns shown in their corresponding flip-angle maps. These artefacts were removed by correcting the RF-gradient time delay for the bipolar spokes (Fig. 5c) or by using the fly-back slice-selective gradient. These were also confirmed by their corresponding flip-angle maps. The EPI images from the fly-back spokes (Fig. 5c), compared with those from bipolar spokes excitations, displayed more intensity drop in regions where B_0 inhomogeneity is known to be severe (eg, above the frontal sinus and the ear canals). This is attributed to the longer pulse duration of the fly-back spokes, which is required to accommodate the rewinding gradient lobes between the subpulses, making these pulses more susceptible to the phase shifts induced by off-resonance. Reductions in flip-angle can also be observed in the same regions in the fly-back spokes pulses' flip-angle maps. Finally, CP-mode EPI images together with their flip-angle maps are also shown in Figure 5e. Compared with the two-spoke excitations, lower signal intensity and lower flip angle can be seen in the CP-mode excitation in the temporal lobes and the cerebellum, confirming the expected benefits of flip-angle homogenization with spokes excitations.

DISCUSSION AND CONCLUSION

In this paper, we provide a mathematical description of the slice-position–dependent excitation errors that occur when there is an undesired delay between a bipolar gradient trajectory and the RF subpulses. These errors are caused by the timing-mismatch–induced phase differences between the subpulses in opposite gradient polarities. The effect is common to all single-channel or parallel transmit excitations that use a bipolar gradient trajectory. Here, it was showcased in the context of bipolar pTx spokes excitations. In all these applications, bipolar trajectories are much preferred over monopolar fly-back schemes because of their significantly greater time efficiency, which reduces excitation pulse duration, alleviates echo time constraints (24), and improves spectral resolution (25).

We furthermore proposed a navigator acquisition that can be used to rapidly estimate the timing mismatch for any desired set of excitation parameters (eg, slice thickness, orientation, and RF bandwidth). The estimated RF-gradient delay was successfully applied back to the bipolar spokes pulses in our modified sequences. In contrast to navigators for readout corrections commonly used in EPI, the excitation errors that we saw here cannot be removed from the images retrospectively. Nonetheless, it is possible to run the navigator described here as a

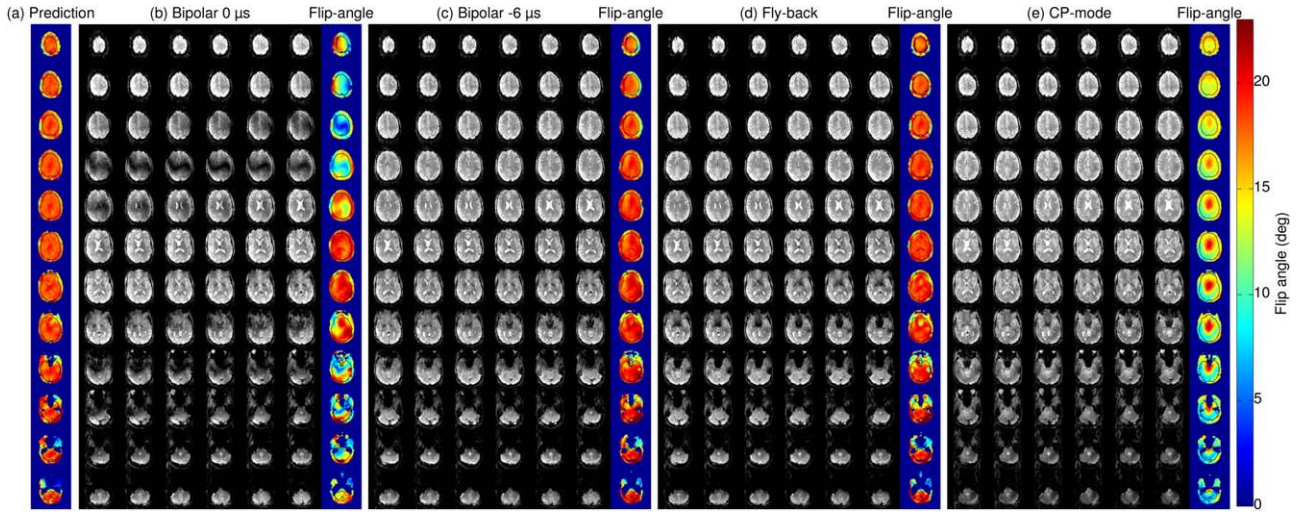

FIG. 5. SMS-spokes-EPI images placed side-by-side with their corresponding excitation flip-angle maps. Two-spoke pulses were designed in a slab-specific fashion for 12 slabs. Six neighboring slices in the EPI protocol were grouped into one slab to share the same spokes pulse. Panel (**a**) is the flip-angle maps predicted from the two-spoke optimization; (**b**) is the SMS-2 bipolar two-spoke EPI without any correction to the relative starting time between RF and slice-selective gradient. Panel (**c**) is the SMS-2 bipolar two-spoke EPI with –6 μs correction to the relative starting time between RF and slice-selective gradient. Panel (**d**) is the SMS-2 fly-back gradient two-spoke EPI. Panel (**e**) is the SMS-2 EPI in CP-mode.

prescan and apply the timing correction directly to the following scans to avoid these excitation errors. Flip-angle maps obtained with PreSat-TFL demonstrate the efficacy of correcting the RF-gradient delay, showing that the intended flip-angle homogeneity can be restored and brought to good agreement with the predicted excitation maps. This translates into improved image quality with bipolar excitations at any off-center slice position, as shown here by in vivo SMS-EPI acquisitions with bipolar 2-spoke SMS-pTX excitations at SMS factor 2.

We also demonstrated that the slice-position–dependent bipolar spokes excitation errors can be mitigated by incorporating the slice-position–dependent phase differences into the spokes pulses according to Equation [4]. If so desired, a combination of the time-shift and phase approach could be used. This may be advantageous if the vendor's hardware control does not allow for sufficient time resolution in the applied time shifts. For example, the majority of the correction can be achieved by adjusting the sequence timing to approximately compensate for the physical timing error, and the residual correction achieved by imposing a small slice-position–dependent phase term. On our scanners, RF timing can be controlled on a 1-μs raster, which, within measurement error, is deemed to be sufficient to achieve good correction.

Instead of a time shift, the excitation errors can be removed by adding extra gradient blips in the slice direction between the subpulses to compensate the gradient moment induced by the RF-gradient delay. This approach is more difficult to implement because of the limited time available for the slice gradient blip solution attributed to the rapid switching of the slice-selective gradient's polarity between the subpulses. Addressing the physical timing error directly by shifting the relative RF-gradient starting time is the most logical and the simplest way to implement without any extra calculation needed.

In summary, an undesired timing delay between the RF subpulses and their bipolar slice-selective gradients lobes was found to be the cause of slice-position–dependent excitation errors observers in bipolar composite pulses. The relationship between the time delay and slice-position–dependent phase errors between the subpulses was described mathematically here and demonstrated experimentally using pTX bipolar spokes excitations. The desired flip-angle homogeneity of the bipolar spokes pulses can be restored by estimating the delay, for example, with the navigator introduced here, and eliminating it by applying the corresponding RF-gradient time shift in the sequence and/or by addition of the corresponding slice-position–dependent phase to the RF subpulses.

ACKNOWLEDGMENTS

We thank Dr Martijn Cloos and Dr Vincent Gras for the valuable discussions on this topic. Scan time supported under Scannexus/Brains Unlimited development project dev_b0_b1 and intramural MBIC funding (project F8015).

REFERENCES

1. Setsompop K, Alagappan V, Gagoski B, et al. Slice-selective RF pulses for in vivo B1+ inhomogeneity mitigation at 7 tesla using parallel RF excitation with a 16-element coil. Magn Reson Med 2008;60:1422–1432.
2. Schmitter S, Wu X, Auerbach EJ, Adriany G, Pfeuffer J, Hamm M, Ugurbil K, van de Moortele PF. Seven-tesla time-of-flight angiography using a 16-channel parallel transmit system with power-constrained 3-dimensional spoke radiofrequency pulse design. Invest Radiol 2014;49:314–325.
3. Tse DHY, Brenner D, Guerin B, Poser BA. High resolution GRE at 9.4T using spokes pulses. In Proceedings of the 23rd Annual Meeting of ISMRM, Toronto, Canada, 2015. p. 546.
4. Tse DH, Wiggins CJ, Poser BA. High-resolution gradient-recalled echo imaging at 9.4T using 16-channel parallel transmit simultaneous multislice spokes excitations with slice-by-slice flip angle homogenization. Magn Reson Med 2017;78:1050–1058.

5. Wu X, Adriany G, Ugurbil K, Van de Moortele PF. Correcting for strong eddy current induced B0 modulation enables two-spoke RF pulse design with parallel transmission: demonstration at 9.4T in the human brain. PLoS One 2013;8:e78078.
6. Zakhor A, Weisskoff R, Rzedzian R. Optimal sampling and reconstruction of MRI signals resulting from sinusoidal gradients. IEEE Trans Signal Proc 1991;39:2056–2065.
7. Jankiewicz M, Zeng H, Moore JE, Anderson AW, Avison MJ, Welch EB, Gore JC. Practical considerations for the design of sparse-spokes pulses. J Magn Reson 2010;203:294–304.
8. Schmitter S, DelaBarre L, Wu X, Greiser A, Wang D, Auerbach EJ, Vaughan JT, Ugurbil K, Van de Moortele PF. Cardiac imaging at 7 Tesla: single- and two-spoke radiofrequency pulse design with 16-channel parallel excitation. Magn Reson Med 2013;70:1210–1219.
9. Zelinski AC, Wald LL, Setsompop K, Goyal VK, Adalsteinsson E. Sparsity-enforced slice-selective MRI RF excitation pulse design. IEEE Trans Med Imaging 2008;27:1213–1229.
10. Davies NP, Jezzard P. Calibration of gradient propagation delays for accurate two-dimensional radiofrequency pulses. Magn Reson Med 2005;53:231–236.
11. Grissom W, Yip CY, Zhang Z, Stenger VA, Fessler JA, Noll DC. Spatial domain method for the design of RF pulses in multicoil parallel excitation. Magn Reson Med 2006;56:620–629.
12. Wu X, Vaughan JT, Ugurbil K, Van de Moortele PF. Parallel excitation in the human brain at 9.4 T counteracting k-space errors with RF pulse design. Magn Reson Med 2010;63:524–529.
13. Duyn JH, Yang Y, Frank JA, van der Veen JW. Simple correction method for k-space trajectory deviations in MRI. J Magn Reson 1998; 132:150–153.
14. Takahashi A, Peters T. Compensation of multi-dimensional selective excitation pulses using measured k-space trajectories. Magn Reson Med 1995;34:446–456.
15. Bernstein MA, King KF, Zhou XJ. Imaging gradients. In: Handbook of MRI Pulse Sequences. Burlington, VT: Academic; 2004:243–273.
16. Shajan G, Kozlov M, Hoffmann J, Turner R, Scheffler K, Pohmann R. A 16-channel dual-row transmit array in combination with a 31-element receive array for human brain imaging at 9.4 T. Magn Reson Med 2014;71:870–879.
17. Tse DHY, Poole MS, Magill AW, Felder J, Brenner D, Jon Shah N. Encoding methods for B1(+) mapping in parallel transmit systems at ultra high field. J Magn Reson 2014;245:125–132.
18. Nehrke K, Versluis MJ, Webb A, Bornert P. Volumetric B1 (+) mapping of the brain at 7T using DREAM. Magn Reson Med 2014;71:246–256.
19. Tse DH, Wiggins CJ, Ivanov D, Brenner D, Hoffmann J, Mirkes C, Shajan G, Scheffler K, Uludag K, Poser BA. Volumetric imaging with homogenised excitation and static field at 9.4 T. Magn Reson Mater Phy 2016;29:333–345.
20. Chung S, Kim D, Breton E, Axel L. Rapid B1 + mapping using a preconditioning RF pulse with TurboFLASH readout. Magn Reson Med 2010;64:439–446.
21. Guerin B, Setsompop K, Ye H, Poser BA, Stenger AV, Wald LL. Design of parallel transmission pulses for simultaneous multislice with explicit control for peak power and local specific absorption rate. Magn Reson Med 2015;73:1946–1953.
22. Sharma A, Bammer R, Stenger VA, Grissom WA. Low peak power multiband spokes pulses for B1 (+) inhomogeneity-compensated simultaneous multislice excitation in high field MRI. Magn Reson Med 2015;74:747–755.
23. Wu X, Schmitter S, Auerbach EJ, Ugurbil K, Van de Moortele PF. A generalized slab-wise framework for parallel transmit multiband RF pulse design. Magn Reson Med 2016;75:1444–1456.
24. Rieseberg S, Frahm J, Finsterbusch J. Two-dimensional spatially-selective RF excitation pulses in echo-planar imaging. Magn Reson Med 2002;47:1186–1193.
25. Yang C, Deng W, Alagappan V, Wald LL, Stenger VA. Four-dimensional spectral-spatial RF pulses for simultaneous correction of B1 + inhomogeneity and susceptibility artifacts in T2*-weighted MRI. Magn Reson Med 2010;64:1–8.

SUPPORTING INFORMATION

Additional supporting information can be found in the online version of this article

Fig. S1. Bloch simulations of the bipolar two-spoke pulses. The same RF and slice parameters as in the 7T imaging experiment (see Methods) were applied in the simulations. The simulations show that without the hardware RF-gradient delay, the expected excitation patterns from the MLS optimization (the left most column in Fig. 3) can be obtained without shifting the relative starting times of the RF and the slice-selective gradient. The minimum NRMSE averaged across all slices is 0.070 at 0 μs time shift.

Fig. S2. 9.4 T PreSat-TFL flip-angle maps of three-spoke pulses measured with a head-shaped phantom. Five slice positions from –32 mm to + 32 mm and including the slice at the isocenter are displayed here. The left column is the predicted flip-angle distribution from the spokes pulse optimization. The second column from the left is the flip-angle maps from the fly-back spokes pulses. The next eight columns are the flip-angle maps from the bipolar spokes pulses with the relative starting time between the subpulses and the slice-selective gradient set from –7 to 0 μs (left to right). The last column is the flip-angle maps from the bipolar spokes pulses with the slice-position–dependent phases corrected using Equation [4] and with the default 0 μs shift in the relative starting time between the subpulses and the slice-selective gradient. The fly-back spokes, the bipolar spokes with –4 μs relative starting time shift, and the bipolar spokes with the slice-position dependent phases corrected agree the best with the prediction.